RESEARCH ARTICLE | OCTOBER 03 2025

Silica-encapsulated MA, Cs, PbX, perovskites via one-pot and post-synthetic routes: Tunable bandgap for white emission and photocatalysis

Sumi Seo [0]; Hyeonyeong Jo [0]; YoonGyo Kim [0]; Eun Young Choi [0]; Soo Jeong Lee [0]; Kayoung Cho [0]; Sohee Mo [0]; You Jeong Lee [0]; Seong Yeon Park [0]; Jin Ho Bang [0]; Iván Mora-Seró [22] [0]; Andrés F. Gualdrón-Reyes [22] [0]; JaeHong Park [23] [0]; Seong Joon Yoon [23] [0]



APL Energy 3, 046101 (2025) https://doi.org/10.1063/5.0283082





Articles You May Be Interested In

A- or X-site mixture on mechanical properties of APbX 3 perovskite single crystals

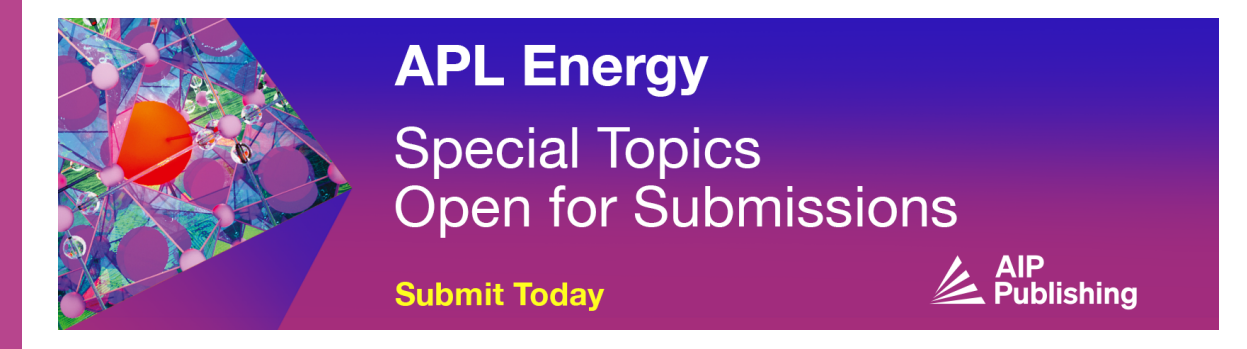
APL Mater. (April 2021)

On the importance of catalysis in photocatalysis: Triggering of photocatalysis at well-defined anatase TiO₂ crystals through facet-specific deposition of oxygen reduction cocatalyst

J. Chem. Phys. (June 2020)

Enhancing photocatalysis in $SrTiO_3$ by using Ag nanoparticles: A two-step excitation model for surface plasmon-enhanced photocatalysis

J. Chem. Phys. (August 2015)





Silica-encapsulated MA_vCs_{1-v}PbX₃ perovskites via one-pot and post-synthetic routes: Tunable bandgap for white emission and photocatalysis 🐵



Cite as: APL Energy 3, 046101 (2025); doi: 10.1063/5.0283082 Submitted: 29 May 2025 · Accepted: 1 September 2025 · **Published Online: 3 October 2025**







Sumi Seo,¹ D Hyeonyeong Jo,¹ D YoonGyo Kim,¹ D Eun Young Choi,² D Soo Jeong Lee,¹ D Kayoung Cho,² Sohee Mo,¹ Vou Jeong Lee,¹ Seong Yeon Park,¹ Jin Ho Bang,^{3,4}

Iván Mora-Seró. 5,a) D Andrés F. Gualdrón-Reves. 6,a) D JaeHong Park. 2,a) D and Seog Joon Yoon 1,a)



AFFILIATIONS

- Department of Chemistry, College of Natural Science, Yeungnam University, Gyeongsan 38541, Republic of Korea
- ² Department of Chemistry and Nanoscience, Ewha Womans University, Seoul 03760, Republic of Korea
- ³ Department of Applied Chemistry, Center for Bionano Intelligence Education and Research, Hanyang University ERICA, 55 Hanyangdaehak-ro, Sangnok-gu, Ansan, Gyeonggi-do 15588, Republic of Korea
- Department of Energy and Bio Sciences, Hanyang University ERICA, 55 Hanyangdaehak-ro, Sangnok-gu, Ansan, Gyeonggi-do 15588, Republic of Korea
- ⁵Institute of Advanced Materials (INAM), Universitat Jaume I (UJI), Avenida de Vicent Sos Baynat, s/n, 12071 Castellón de la Plana, Castellón, Spain
- Facultad de Ciencias, Instituto de Ciencias Químicas, Universidad Austral de Chile, Isla Teja, Valdivia 5090000, Chile

Note: This paper is part of the Special Topic Applied Energy in Latinoamerica.

^{a)}Authors to whom correspondence should be addressed: sero@uji.es; andres.gualdron@uach.cl; jaehong@ewha.ac.kr; and yoon@yu.ac.kr

ABSTRACT

Halide perovskites (HPs) with various dimensional variations have been established as potential materials for fabricating efficient solar light conversion systems, display devices, and thin-film transistors, as well as prominent photocatalysts to trigger solar-driven applications. However, to practically use HPs and focus efforts on their prominent commercialization, degradation mechanisms and strategies for enhancing material stability and device operating durability are being widely studied. In this contribution, an amorphous silica-covered perovskite quantum dot (PQD) structure has been studied to understand (i) the formation mechanism of $MA_vCs_{1-v}PbX_3@SiO_x$ and their halide exchange processes during the synthetic or post-synthetic stage, and (ii) the effect of a non-stoichiometric A-site/X-site ion composition on the photoexcited electron recombination dynamics in the MA_yCs_{1-y}PbX₃@SiO_x PQDs. Through the modification of the ligand-assisted reprecipitation $synthetic \ methods \ of the \ conventional \ CsPbBr_3@SiO_x \ to \ obtain \ multi-colored \ MA_yCs_{1-y}PbX_3@SiO_x, the \ color \ gamut \ is \ comparable \ to \ the$ Rec. 2020 standard—up to 93.55%—with more pristine blue/red emissions. In addition, these PQDs@SiO_x can facilitate the photocatalytic (PC) oxidation of benzyl alcohol in ethanol via chemisorption through Si-OH silanol groups, reaching a photodegradation efficiency of ~35%. This work demonstrates the versatile potential of PQDs to be used in display technologies and to perform PC reactions in polar solvents.

© 2025 Author(s). All article content, except where otherwise noted, is licensed under a Creative Commons Attribution-NonCommercial 4.0 International (CC BY-NC) license (https://creativecommons.org/licenses/by-nc/4.0/). https://doi.org/10.1063/5.0283082

I. INTRODUCTION

Recent advances in halide perovskite (HP) processing to perform solar-driven chemical reactions (e.g., hydrogen production, organic degradation2), to fabricate display technologies,2 and lasing,3 among others, have generated growing attention, considering their impressive intrinsic features such as a high absorption coefficient,4 good carrier transport ability,5 controllable surface chemistry,6 and low-cost synthesis.7 Certainly, composition engineering and nanoconfinement have opened the door to enhancing the photophysical properties of HPs (now in the form of quantum dots, QDs),8 generating a less-defective structure and modulating their band structure and bandgap across a broad range of the electromagnetic spectrum. In this context, one of the most successful strategies to modify the optical features of perovskite QDs (PQDs) is through a post-synthetic halide exchange process, 9,10 where the color gamut of PQDs can be expanded more than 30% of the NTSC TV color standard displayable area, with a notable 15–30 nm full-width at half-maximum (FWHM) of the emission peak. This demonstrates the remarkable emission quality and purity from these photomaterials. Therefore, it is worth noting the achievement of important breakthroughs in optoelectronics and emerging photovoltaics, such as the fabrication of multicolor light-emitting diodes with external quantum efficiencies of up to 30%, 11,12 and PQDs-based solar cells with photoconversion efficiencies near to 20%. 13

Beyond preparing high-quality PQDs, their limited stability has been the main reason hindering both their commercialization and future scaling of HP-based devices.¹⁴ To increase the PQD stability against humidity and oxygen, coverage of PQDs using SiO_x, ^{15–17} CdS, ¹⁸ SiO₂-Al₂O₃, ¹⁹ NaNO₃, ²⁰ polymeric matrices, ^{21,22} etc., has been explored. In this way, previous studies performed in our research group exhibit the synthesis of CsPbBr3 PQDs in an amorphous silica medium under ambient conditions at room temperature using the ligand-assisted reprecipitation (LARP) method. Here, the PQDs@SiO_x formation mechanism is highlighted based on the emergence of -Si-O-Si-linkages influencing the PQDs core sizes,²³ and the ultrafast photoexcited carrier dynamics in the PQDs@SiO_x system, where electron-hole separation is induced between the silica medium (electrons) and PQD core (holes) in around 2 ns.²⁴ According to these studies, it is possible to promote the growth of PQD cores within 1-2 s of reaction, originating from fast agglomeration of the lead halide plumbate precursor,²⁵ but this process also favors the emergence of a Cs-deficient composition, inducing the introduction of Pb into Cs positions (also known as interstitial defects, Cs_{Pb}). The presence of Cs^+ defects promotes the appearance of intraband carrier energy traps, assisting the non-radiative recombination dynamics in the perovskites, which quenches their PL properties.² Thus, it is imperative to find a prominent alternative to compensate for the Cs⁺ defects in the PQDs@SiO_x, with the purpose of improving the radiative recombination and color quality of nanoparticles for further application.

In this work, we modified the LARP process for the synthesis of PQDs embedded in a silica medium by introducing methylammonium halides (MAX, X = Cl⁻, Br, I⁻) during LARP synthesis or post-synthetic anion exchange to produce MA_vCs_{1-v}PbX₃@SiO_x. First, the incorporation of MA+ cations favors the filling of Cs+ defects in the CsPbBr₃@SiO_x PQDs, which contributes to increasing the PLQY and radiative recombination constant of the photoactive material by 2 times. This indicates that MA+ can provide radiative channels to influence the carrier recombination dynamics in the perovskite, improving its optical performance.²⁷ Furthermore, the addition of MAX allows extension of the color gamut by introducing Cl⁻ or I⁻ anions into the main CsPbBr₃@SiO_x structure, modulating the bandgap of the resulting perovskite. Furthermore, a post-synthetic annealing process was applied to the resultant materials to induce silica coverage hardening,²³ delaying the interdot halide exchange process to produce white light emission after mixing blue-, green-, and red-colored MA_vCs_{1-v}PbX₃@SiO_x. Finally, PQDs@SiOx were used as photocatalysts for the photocatalytic (PC) oxidation of benzyl alcohol (BzOH), with an efficiency of ~35% under UV-Vis illumination in an ethanol (EtOH) environment. This contribution offers insight into the impact of A-site cation deficiency on the photophysical properties of MA_vCs_{1-v}PbX₃@SiO_x, which show potential application in display technologies and polar-solvent-mediated PC chemical reactions.

II. RESULTS AND DISCUSSIONS

A. Synthetic and post-synthetic red, green, and blue $MA_{\nu}Cs_{1-\nu}PbX_{3}@SiO_{x}$ PQDs

To induce both bandgap tunability and a wide color gamut, a modified LARP process was carried out, incorporating MACl or MAI in an anti-solvent as shown in Fig. S1(A), producing luminescent multicolor $MA_yCs_{1-y}PbX_3@SiO_x$ colloidal suspensions. Figure 1(A) depicts the UV–Vis absorption and PL spectra of $MA_yCs_{1-y}PbX_3$ PQDs in a silica medium by varying halide compositions $(MA_yCs_{1-y}PbCl_{3-x}Br_x, MA_yCs_{1-y}PbBr_3,$ and $MA_yCs_{1-y}PbBr_{3-x}I_x$, hereafter named as Blue, Green, and Red PQDs

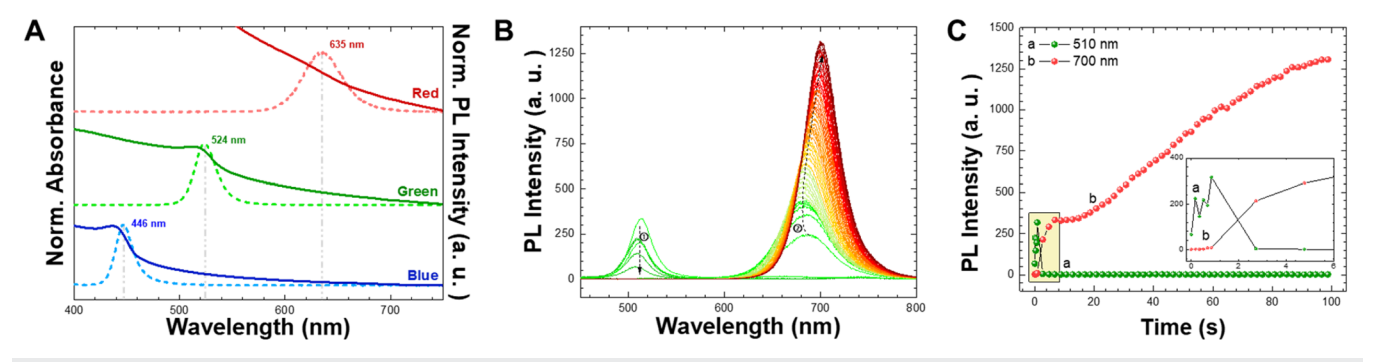


FIG. 1. (A) UV–Vis. absorption spectra (straight line) and PL spectra (dotted line) of MA_yCs_{1-y}PbX₃ PQDs in a silica medium with the addition of the MAX while in the LARP process. (B) With the addition of the MAI in the anti-solvent, *in situ* PL spectra of the MA_yCs_{1-y}PbX₃ PQDs in a silica medium during the formation of the PQD cores in the LARP process. (C) Time-dependent *in situ* PL intensity kinetic profiles of the MA_yCs_{1-y}PbX₃ PQDs during the formation (green and red dots for emission at 510 and 700 nm, respectively). Inset (C) presents the PL intensity changes at earlier times up to 6 s.

in this work, respectively). The corresponding PL peak positions for the PQDs@SiO $_x$ (~446, 524, and 635 nm, for blue, green, and red emission, respectively) appeared with narrow FWHMs (~20, 30, and 40 nm for blue, green, and red, respectively), exhibiting a 5 nm Stokes shift from their respective absorption excitonic peaks. Then, by varying the amount of MACl or MAI in the anti-solvent for the LARP process, the PL peak positions of MA $_y$ Cs $_{1-y}$ PbX $_3$ @SiO $_x$ PQDs can be modulated from 416 to 740 nm, covering the entire visible color emissions; see Figs. S1(B)–S3.

By conducting in situ PL spectroscopy during PQD formation in the silica medium, as shown in Figs. 1(B) and 1(C), a consequent PL appeared first around 500 nm within 1 s, while the PL intensity around 700 nm increased up to 100 s. As reported previously,²³ the appearance of PL around 500 nm in 1 s is ascribed to the emergence of CsPbBr3 PQD cores. By carefully monitoring in situ PL spectra at earlier times [Fig. 1(C), inset], correlated initial PL at 500 nm decreased, and PL around 700 nm evolved simultaneously. The simultaneous PL redshift phenomena can be explained as (i) the formation of CsPbBr3 PQDs (<1 s) and (ii) subsequent formation of red-colored $MA_{v}Cs_{1-v}PbBr_{3-x}I_{x}$ PQDs with halide exchange between the CsPbBr₃ PQD cores and MAI in the anti-solvent through the silica medium, up to 100 s. In the LARP synthetic procedure, the reaction between CsBr and PbBr₂ first produces lead bromide plumbate, then mixed precursors (CsBr, PbBr₂, APTES, and EG) were added into the anti-solvent with MAI (see details in the Experimental Section). Kinetically, we anticipated the formation of CsPbBr₃@SiO_x and then the consequent halide exchange occurred between the CsPbBr3 PQD cores and MAI in the mixture reaction. Here, imperfect silica coverage onto the PQDs could induce intermolecular interactions, such as electron or hole transfer, electrochemical oxidations, and so on. 23,24,28,29 In addition, in the absence of a post-synthetic annealing process, polar solvents such as DMF, acetone, etc., can permeate through imperfect silica coverage to reach the PQD core and favor degradation occurrence.²⁵ In this context, the interfacial halide exchange reaction takes place over tens of seconds or longer,³⁰ so overall results supported that the kinetically favored CsPbBr₃ PQD core (around 0.1–1 s⁻¹) formation occurred first and then, for a longer reaction, halide exchange $(\sim 10^{-2} \text{ s}^{-1})$ triggers the appearance of MA_vCs_{1-v}PbX₃ PQDs in the

To support the kinetically favored CsPbBr₃ PQD formation and subsequent Green and Blue MA_vCs_{1-v}PbX₃ PQD occurrence in the silica medium, Fig. S4 shows in situ PL spectra, highlighting emission changes by monitoring the corresponding PL intensities for CsPbBr₃/Green/Blue PQDs, and estimating their formation rates obtained through peak position changes. Similar trends in both Green and Blue MA_vCs_{1-v}PbX₃ PQD@SiO_x are shown in Fig. 2, where the initial PL for the CsPbBr₃ PQDs occurred within 1 s, and then, a consequent peak position shift happens (up to 525 nm or 460 nm, for Green or Blue PQDs, respectively). A similar $MA_vCs_{1-v}PbX_3$ PQD formation rate $(8.5 \times 10^{-2} \text{ and } 3.6 \times 10^{-2} \text{ s}^{-1})$ for Green and Blue PQDs, respectively; see Fig. S4) supports the subsequent formation of CsPbBr₃ and MA_vCs_{1-v}PbX₃ PQDs. Another possibility of bandgap tuning for MA_vCs_{1-v}PbX₃ PQDs in the silica medium is promoted through the post-synthetic halide exchange process, by mixing the MA_vCs_{1-v}PbX₃ PQD suspension with the MAX solution. Without applying the post-synthetic annealing process, the molecules or ions in the solution can reach the PQD cores

by permeating the imperfect silica coverage. ^{23,25,28,29} As shown in Figs. 2 and S5, most of the halide exchange processes, especially from a smaller halide [from Br to Cl, see Figs. 2(A) and 2(B)] to a bigger one [from Br to I, see Figs. 2(C) and 2(D)], could be observed through *in situ* PL spectroscopy while the halide exchange process occurred. With a range of around 10^{-1} – 10^{-2} s⁻¹ exchange rates, post-synthetic halide exchange also occurred up to 100 s, similar to the direct formation of MA_yCs_{1-y}PbX₃ PQDs in the LARP process, see Fig. 1. In this way, Figs. 1 and 2 demonstrate that the bandgap modulation can be led through divalent synthetic and post-synthetic MA_yCs_{1-y}PbX₃@SiO_x PQDs for a wide color gamut.

B. Surface and photophysical properties of the $MA_vCs_{1-v}PbX_3$ PQDs@SiO_x

Through material characterizations, compositional changes and the formation of different crystalline structures were able to be tracked. High-resolution (HR) XPS spectra for each composition of PQD@SiO_x and their analysis were demonstrated in Figs. 3, S6, and S7. It was observed that the MAX incorporation into the Cs-deficient CsPbBr3 crystalline PQDs induces the formation of the Red/Green/Blue MA_yCs_{1-y}PbX₃@SiO_x PQDs. Through HR-XPS spectra of elements such as halides, Pb, Cs, and NH₃⁺ from the A-site cation composition in the perovskite, the corresponding stoichiometric compositions were estimated and shown in Fig. 3(A). For CsPbBr₃@SiO_x, a non-stoichiometric composition for Cs and Br was calculated. The Cs-deficient composition in the perovskite structure was one of the negative aspects of the perovskite made through the conventional LARP process.³² However, through the modified LARP synthetic route, A-site cation: B-site metal cation:halide ratios for Red, Green, and Blue PQDs are 0.79:1:3.47, 0.90:1:2.86, and 0.78:1:2.57, respectively. In contrast, the estimated ratio for CsPbBr₃ PQDs was 0.11:1:1.11. Accordingly, it is deducible that the incorporation of MAX into the CsPbBr3 cores increases the relative A-site cation and halide composition in the ABX3 perovskite structures to significantly compensate for the expected stoichiometric ratio,³³ compared to the compositional ratio of the initial CsPbBr3 core. As shown in Fig. 3(B), there are two possible components, originated from APTES (amine and ammonium species for the two peaks in ~398-401 eV)³⁴ for the CsPbBr₃@SiO_x PQDs, while for the mixed cation PQDs, it is possible to achieve the typical signal for -NH₃⁺ from MA⁺ in MAPbX₃ perovskites ~400 eV. 35 Note that the deconvoluted peak area for -NH₃⁺ from MAPbX₃ perovskites was used to calculate elemental ratios by dividing each atomic sensitivity factor (ASF). The presence of MA⁺ also supports its incorporation into the PQD cores to form MA_vCs_{1-v}PbX₃ PQDs in the silica medium. In Figs. S6 and S7, minor peaks for unreacted species (PbBr₂ or CsBr) or interstitial Pb⁰ were detected, ³⁶ but most of the signals are attributed to perovskite and silica components with their oxidation/reduction ionic forms.

With the purpose of obtaining information about the crystalline structure of photoactive materials, XRD patterns of the CsPbBr₃@SiO_x and Blue/Green/Red MA_yCs_{1-y}PbX₃@SiO_x PQDs were presented, see Fig. S8. First, the XRD peaks of CsPbBr₃@SiO_x PQDs were ascribed to the typical crystal planes of the orthorhombic phase (ICSD 97851),³⁷ while the XRD peaks of MA_yCs_{1-y}PbCl_{3-x}Br_x@SiO_x and MA_yCs_{1-y}PbBr₃@SiO_x PQDs correspond to the cubic phase (ICSD 252415).³⁸ At this point,

APL Energy ARTICLE pubs.aip.org/aip/ape

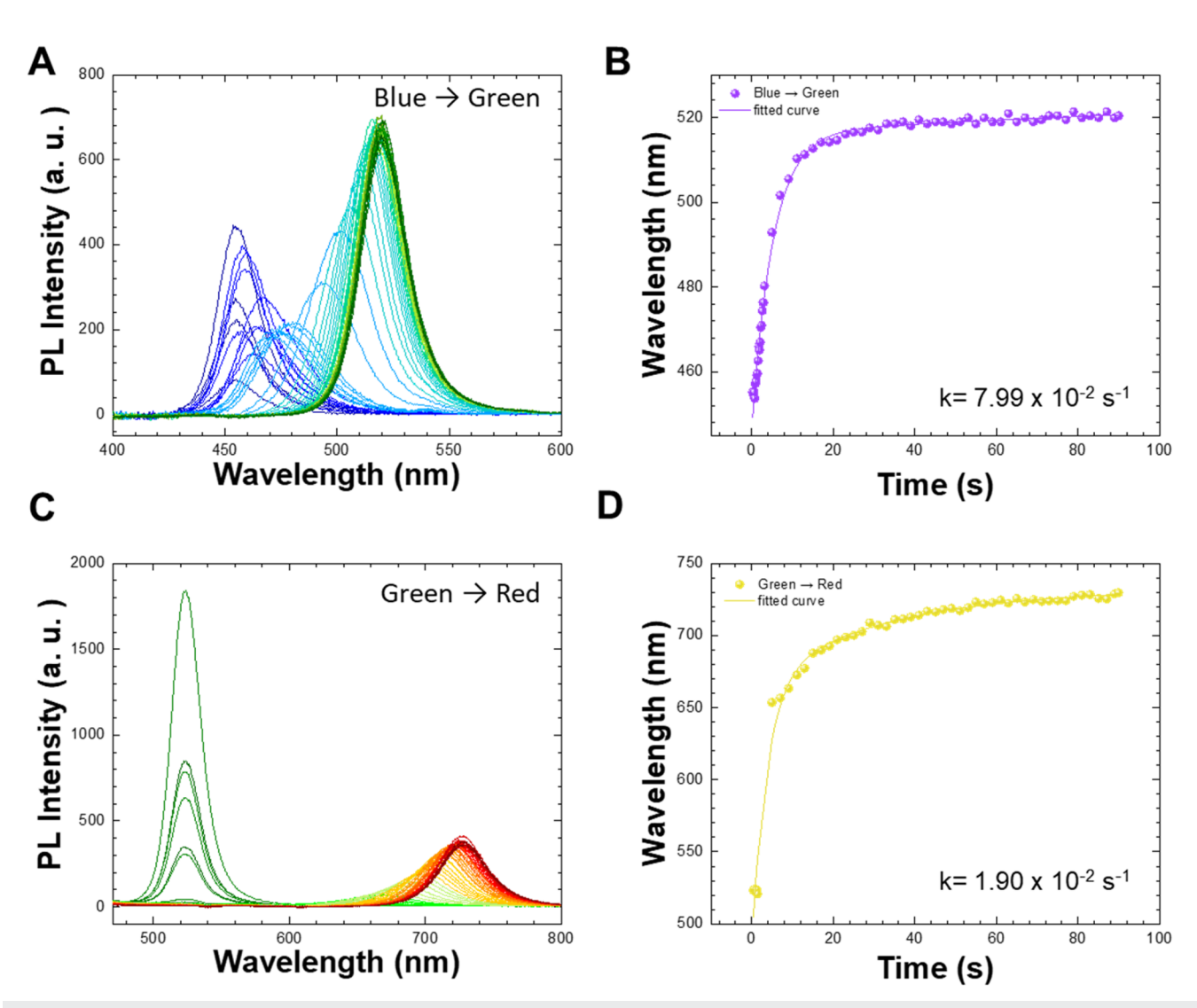


FIG. 2. (A) and (C) Time-dependent *in situ* PL spectra and (B) and (D) PL peak position changes over 100 s during the post-synthetic halide exchange process. After making MAy₂Cs_{1-y}PbX₃ PQDs [(A) and (B): Blue PQDs, (C) and (D): Green PQDs] in a silica medium through the LARP process, counter MAX [(A) and (B): MABr, (C) and (D): MAI] were dissolved in additional anti-solvent, and the PQDs@SiO_x were mixed and stirred to introduce the post-synthetic halide exchange. (B) and (D) The kinetics of the peak positions were fitted through an empirical pseudo-first-order kinetic analysis, as $y = y_0 + A \cdot \exp(-x/\tau)$, where y, y_0, A, x , and τ represent PL peak positions, initial PL peak position, amplitude, time, and lifetime of growth kinetics, respectively.³¹

the orthorhombic-to-cubic phase conversion after adding MABr and MACl allows us to suggest the reduction of lattice distortion of the perovskite through compensation of Cs⁺ and X⁻ defect sites, obtaining a more symmetric perovskite lattice. Conversely, the XRD profile of MA_yCs_{1-y}PbBr_{3-x}I_x@SiO_x PQDs is attributed to the tetragonal phase (ICSD 241480),³⁸ indicating that the introduction of iodide species with higher lability compared with Br– and Cl– anions (after MAI addition) can favor a stronger octahedral deformation,³⁹ which induces the orthorhombic-to-tetragonal phase conversion. The nature of the halide also has a pivotal effect on the particle size of the MA_yCs_{1-y}PbX₃@SiO_x PQDs, where the

Blue, Green, and Red PQD core diameters were determined to be 4.1 \pm 0.8, 6.4 \pm 1.2, and 7.9 \pm 0.9 nm, respectively (see Fig. S9). Thus, it is deducible that the bigger the halide composing the perovskite core (I $^-$ > Br $^-$ > Cl $^-$), the bigger the PQD size, lowering the nanoconfinement effect. This fact favors a higher degree of perovskite lattice deformation, which agrees with the emergence of the low-symmetric tetragonal crystalline phase for $MA_yCs_{1-y}PbBr_{3-x}I_x@SiO_x$ PQDs. Following our earlier study, 23 and independent of the post-synthetic annealing process, FT-IR spectra in Fig. S10 depict vibrations from the silica medium: C–H vibration (2921 and 3022 cm $^{-1}$), C=C vibrations (1604 cm $^{-1}$), and

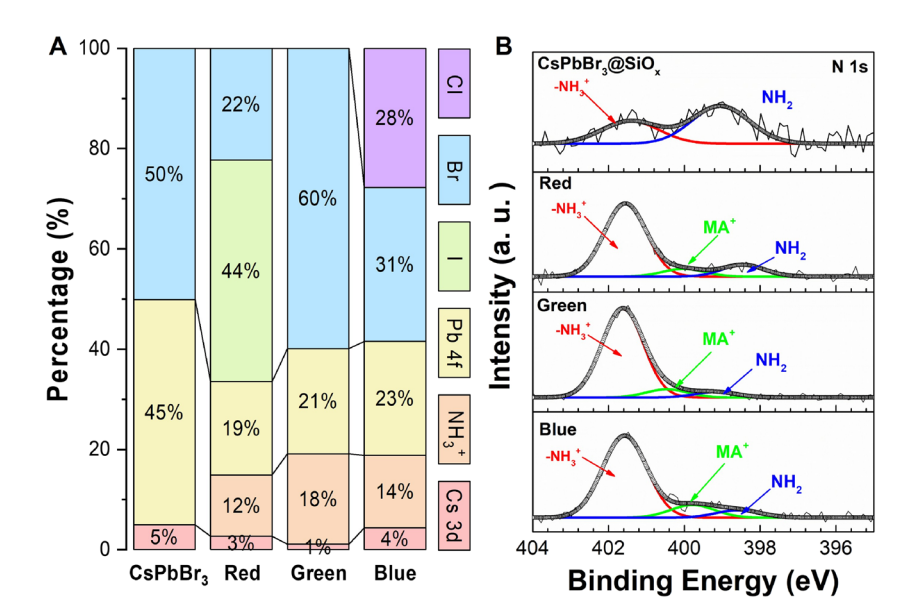


FIG. 3. (A) Relative elemental compositions (Cl, Br, I, Pb, NH3+, and Cs) of the $CsPbBr_3$ or $MA_yCs_{1-y}PbX_3$ PQDs (Red, Green, and Blue PQDs) in a silica medium obtained through their XPS analysis. (B) High-resolution XPS spectra of the N 1s for the CsPbBr₃ or $MA_yCs_{1-y}PbX_3$ PQDs (Red, Green, and Blue PQDs) in a silica medium and their deconvoluted peaks with their assignments.

Si-O-Si (1084 and 1027 cm⁻¹). In addition, NH₃⁺ vibrations at 1494 cm⁻¹ (bending vibration), and 731, and 691 cm⁻¹ (asymmetric bending vibrations) were also found. The NH₃⁺ vibrations can be found from the MAPbX₃ bulk layered structure. 40,41 In short, the addition of MAX during the LARP process impacted the core crystalline structure by the addition of MA+ into the Cs-deficient sites to resemble cubic MA_vCs_{1-v}PbCl_{3-x}Br_x/MA_vCs_{1-v}PbBr₃ and tetragonal MA_vCs_{1-v}Br_{3-x}I_x PQD structures, compensating the stoichiometric compositions.

To monitor the effect of MAX incorporation into the Csdeficient CsPbBr3 core on the photophysical properties of the PQDs@SiO_x, fs-TAS was performed, and the difference absorbance spectra with kinetic profiles were presented in Fig. 4. The groundstate bleaching (GSB) of the CsPbBr₃@SiO_x appeared around 510 nm, and GSB for the Green MA_vCs_{1-v}PbBr₃ @SiO_x PQDs was shown around 540 nm, corresponding to the red shift phenomenon of the PL maxima (see Fig. S4). In contrast, the GSB for the Blue PQDs@SiO_x appeared around 480 nm due to the subsequent halide exchange from Br to Br/Cl mixed halide form in the PQDs during the modified LARP process. The decays of GSB in Figs. 4(A)-4(C) present the photoexcited charge recombination at the band edge. Note that the negative ΔA elongated to 800 nm in Figs. 4(B) and 4(C) could originate from scattering of the probe light by passing through the amorphous silica medium.

The normalized kinetic profiles of the GSBs for CsPbBr₃@SiO_x and Green/Blue PQDs and their empirical bi-exponential decay fitting traces were presented in Fig. 4(D). As shown in the inset in Fig. 4(D), most of the traces decreased within 200 ps, but there were longer decay components in all cases of the CsPbBr₃@SiO_x and Green/Blue PQDs. The faster decay and longer decay components correspond to carrier trapping and radiative carrier recombination, respectively.⁴² Detailed parameters obtained through the bi-exponential decay fitting process, 43,44 average lifetime of the decay

 (τ_{avg}) , PLQYs, and radiative/non-radiative recombination decay rate constants (k_r and k_{nr} , respectively) were presented in Table I. Note that PLQY was obtained separately by measuring absolute PLQY values in each CsPbBr₃@SiO_x and Green/Blue PQDs@SiO_x (see details in the Experimental Section). In comparison to Green PQDs@SiO_x and CsPbBr₃@SiO_x, the carrier trapping in the Green PQD core took around 1.5 times longer than in the CsPbBr₃ PQD core, even though other components were similar. On the other hand, PLQY for the Green PQDs@SiOx was about 2 times higher than the PLQY for the CsPbBr₃@SiO_x PQDs. Due to the aforementioned slower carrier trapping and higher PLQY, we estimate the calculated k_r for the Green PQDs@SiO_x, which is around 2 times higher than that for the CsPbBr₃@SiO_x, even though the k_{nr} for both cases was similar. Here, it is deducible that the introduction of MABr species into the CsPbBr₃ structure promotes the passivation of Cs⁺ defect sites by the presence of MA⁺ cations and simultaneously, the compensation of Br vacancies, lowering the density of nonradiative carrier traps in the resulting Green PQD core [lower carrier trapping rate $(k_1 = 1/\tau_1)$] and favoring the emergence of radiative channels to influence the carrier recombination dynamics. On the other hand, since Blue PQDs@SiOx present faster carrier trapping with a larger amplitude (A_1), the overall τ_{avg} for Blue PQD@SiO_x is about 3% of that for the Green PQD@SiOx or CsPbBr3@SiOx. At this point, we suggest that although the MACl source can compensate Cs⁺ vacancies in the initial CsPbBr₃ PQD core, improving the radiative recombination pathway, Cl species are also known to create intrabandgap deep states, increasing the likelihood of nonradiative recombination mechanisms in the resulting Blue PQD core, compared with pristine CsPbBr₃ or Green PQDs ones (a higher $k_{\rm nr}$). Accordingly, we conclude that the introduction of MABr produces an efficient surface compensation of Cs+ and X- vacancies in the CsPbBr₃@SiO_x PQDs, enhancing the optical performance of MA_xCs_{1-v}PbBr₃@SiO_x PQDs.

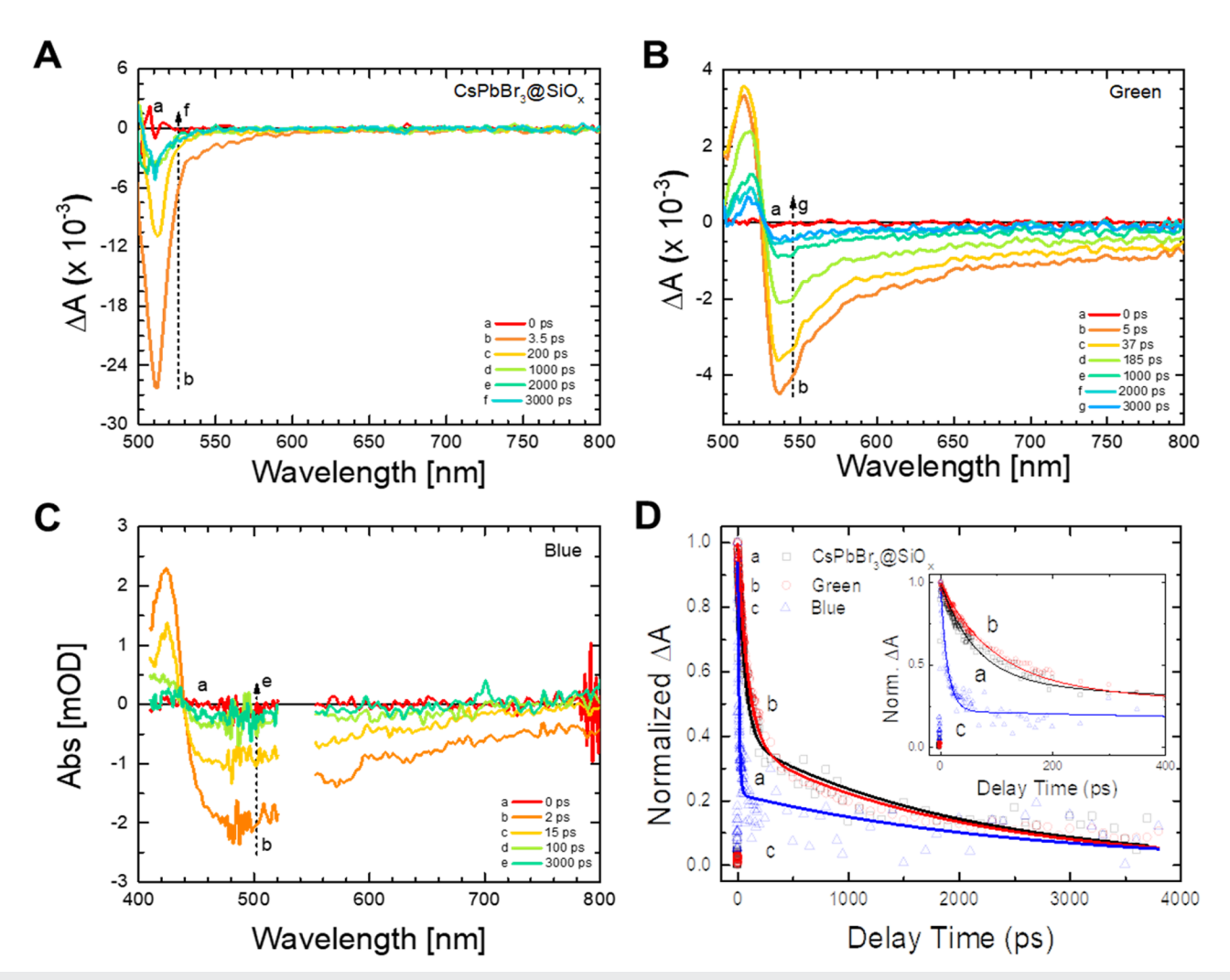


FIG. 4. Time-resolved differential absorption spectra of (A) CsPbBr₃, and (B) and (C) MA_yCs_{1-y}PbX₃ PQDs [(B) and (C), for Green and Blue PQDs, respectively] in the silica medium obtained through TA spectroscopic measurements. (D) Normalized ground-state bleaching decay kinetic profiles (CsPbBr₃@SiO_x: 510 nm; Green: 535 nm; Blue: 480 nm) with bi-exponential decay fitting curves (inset: enlarged kinetic profiles up to 400 ps).

TABLE I. Determination of radiative and non-radiative recombination decay rate constants, $k_{\rm f}$ and $k_{\rm nr}$, respectively, by fitting the normalized TA kinetic profiles of CsPbX₃, Green, and Blue PQD@SiO_x through a bi-exponential function $\Delta A = y_0 + A_1 e^{-x/\tau_1} + A_2 e^{-x/\tau_2}$, 46 shown in Fig. 4(D). Expressions used in the calculations: $\tau_{\rm avg} = \frac{\sum A_1 \tau_1}{\sum A_j}$, $\tau_{\rm avg} = \frac{1}{k_r + k_{\rm nr}}$ and $(PLQY) = \frac{k_r}{k_r + k_{\rm nr}}$. PLQY values were used in the 0–1 range.

Perovskite	A_1	$\tau_1 \times 10^1 \; (ps)$	A_2	$\tau_2 \times 10^3 \; (ps)$	$T_{avg}\times 10^2~(ps)$	PLQY (%)	$k_{\rm r} \times 10^7 \; ({\rm s}^{-1})$	$k_{\rm nr} \times 10^9 \; ({\rm s}^{-1})$
CsPbBr ₃ @SiO _x	0.61	6.26	0.39	2.00	8.20	1.77 ± 0.64	2.16	1.20
Green	0.63	9.29	0.37	1.97	7.88	3.33 ± 0.74	4.22	1.23
Blue	0.78	1.23	0.22	2.60	0.26	2.86 ± 0.63	4.92	1.67

C. Expansion of the color gamut of the $MA_yCs_{1-y}PbX_3$ PQDs@SiO $_x$ with divalent white color emissions for display and photocatalysis

To utilize divalent $MA_yCs_{1-y}PbX_3$ PQDs@SiO_x for display and photocatalysis applications, by carefully tuning PL in the entire

visible range, the color gamut of the $MA_yCs_{1-y}PbX_3$ PQDs@SiO_x was demonstrated in Fig. 5(A). Compared to standard color gamuts, the color gamut of the $MA_yCs_{1-y}PbX_3$ PQDs@SiO_x presents similar or better performance (93.55%, 131.8%, and 178.6% vs Rec. 2020, Adobe, and sRGB, respectively). In addition, by utilizing the post-synthetic annealing process (see details in the Experimental Section),

APL Energy ARTICLE pubs.aip.org/aip/ape

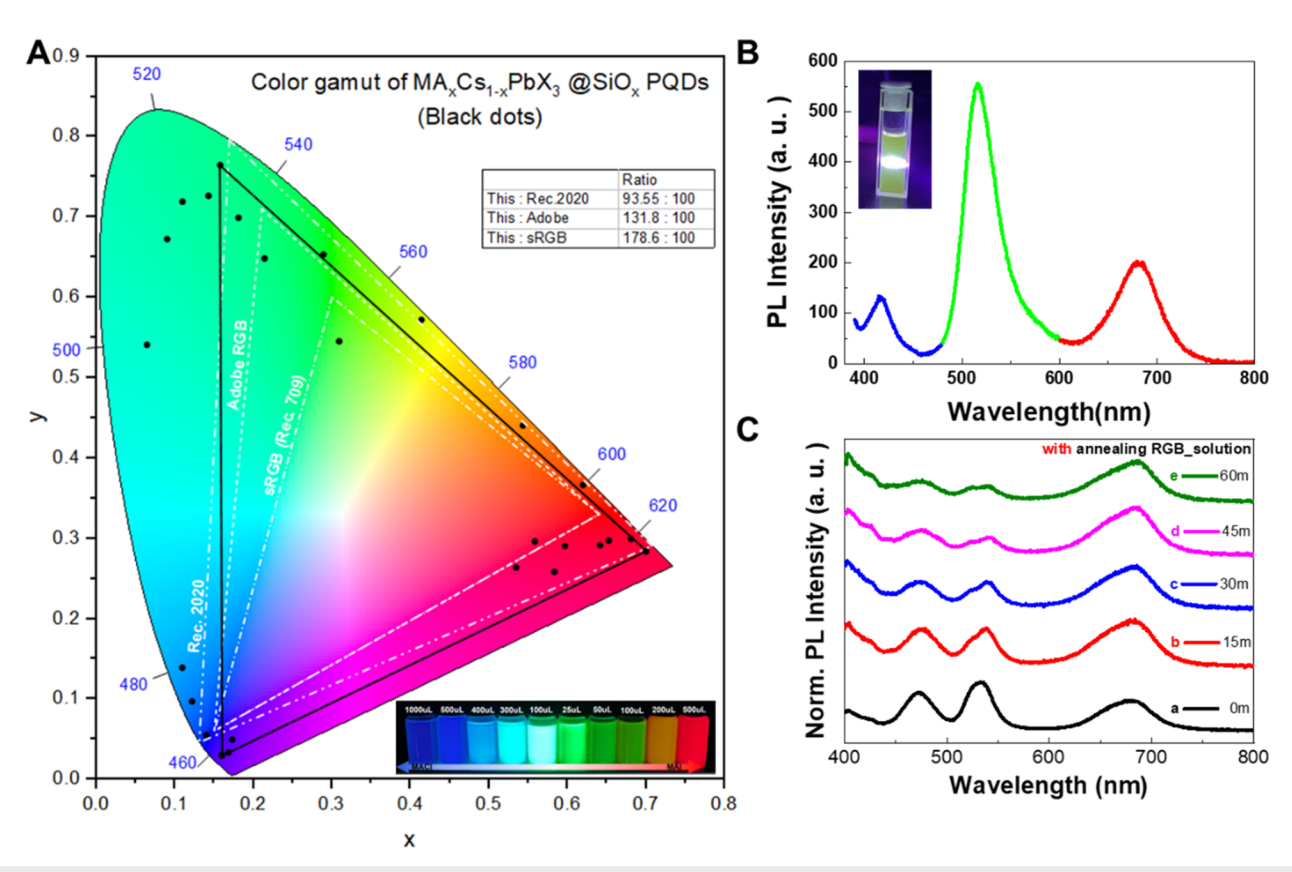


FIG. 5. (A) CIE chromaticity diagram of MA_yCs_{1-y}PbX₃ PQD in a silica medium by modulating various halide compositions. The regions for the standard Rec. 2020, Adobe, and sRGB are presented as white dashed triangles. The inset photograph in Fig. 5(A) presents a corresponding luminescent photograph of the PQD suspensions by varying the MAX compositions. (B) A PL spectrum of the Red, Green, and Blue mixed PQD@SiO_x suspension with their white emission in the inset photograph. (C) Time-dependent PL spectra at every 15 min for the Red, Green, and Blue mixed PQD@SiO_x suspension, with the post-annealing process applyied after the LARP synthetic process.

the Blue/Green/Red suspension was able to be mixed to generate white color emission, see Fig. 5(B). The post-synthetic annealing process introduces silica shell hardening to form the amorphous SiO_x , increasing the PQD stability against H_2O , as reported earlier.²³ As shown in Figs. 5(C) and S11, we were able to observe, through PL measurements under ambient conditions with constant 1 sun illumination, that the thermal treatment of MA_vCs_{1-v}PbX₃@SiO_x PQDs enables the perovskite mixture to maintain the white emission for up to 60 min. Nevertheless, without the annealing process, the white emission disappeared after 15 min. This difference can also be observed through the estimation of the kinetic constant (kc) of PL intensity quenching for each Blue, Green, and Red component in the respective PQD mixtures, with and without annealing, see Figs. S12(A) and S12(B), where the thermally treated PQDs show a longer k_c compared with the non-annealed ones. This allows us to deduce that most of the pores from the SiO_x covering the PQDs are sealed under post-synthetic annealing, hindering the halide exchange between the perovskite nanoparticles.²³ On the other hand, we analyzed the luminescence of the Blue, Green, and Red MA_yCs_{1-y}PbX₃@SiO_x PQD films, after applying the post-synthetic annealing process and storing at 85 °C and 85%

relative humidity (RH), with the purpose of observing their PL stability under practical conditions. Here, the white light emission of the annealed PQD mixture is rapidly quenched, suggesting that one of the RGB components deteriorates. Accordingly, we studied the PL stability of individual annealed Blue, Green, and Red PQD films separately under the above temperature/RH atmosphere for 80 min, see Figs. S13(A)-S13(C), where the Red PQDs exhibit the fastest PL intensity lowering. This behavior is ascribed to material degradation, considering that the iodide-PQDs are prone to suffer a high degree of lattice distortion by the formation of iodide defects when bulk material is formed.³⁹ Thus, Red PQDs can retain ~40% of the relative PLQY, while Blue and Green PQDs can maintain ~70%, see Fig. S13(D). Accordingly, the balance between the PL intensity of RGB components cannot be kept, explaining the fast quench of white light emission under practical conditions. Finally, by introducing an arbitrary combination of Blue, Green, and Red PQDs@SiOx suspensions, it was possible to demonstrate bluish, greenish, and reddish white emissions with their PL spectra, see Fig. S14. Taking advantage of the luminescent features of these PQDs, these materials were deposited as active layers on commercial blue LEDs, achieving colorconverting devices. Here, we obtained their respective PL features of 06 October 2025 11:44:19

Blue, Green, and Red LEDs at 480, 539, and 687 nm, respectively, under operation at 2.5 V for 1 min, see Figs. S15(A)–S15(C), which is also denoted in their chromaticity coordinates, see Fig. S15(E). On the other hand, the mixture of PQDs and subsequent deposition on blue LEDs mediates the emergence of white emission, see Fig. S15(D). However, its PL emission could not be detected, indicating that a low luminescence is provided. In this context, we are studying prominent alternatives to cover the PQDs with the aim of extending the PL stability for a long term and improving the PL emission of the LED devices. Despite this scenario, we show that it is possible to employ our $MA_yCs_{1-y}PbX_3@SiO_x$ PQDs as an initial stage in the fabrication of color-converting LEDs.

After analyzing the intrinsic properties of the APbX₃@SiO_x PQDs, we proceeded to observe their photocatalytic (PC) properties in polar media. We performed the PC oxidation of benzyl alcohol (BzOH) as a target molecule in ethanol (EtOH), monitoring its characteristic UV–Vis absorption spectrum (maximum peak at 258 nm) in the absence [Fig. 6(A)] and presence of PNC-based photocatalysts under continuous UV–Vis light illumination for 100 min, see Figs. 6(B)–6(D). We carried out this PC reaction in EtOH since the SiO_x shell hinders the close interaction between polar molecules and perovskites, allowing us to study their PC capability in harsh conditions. ^{47,48} The change in the absorbance of BzOH was denoted as A/A_0 [see Fig. 6(E)], where A_0 is the initial absorbance of the molecule and A is the absorbance as a function of time. Then, the

corresponding pseudo-first-order rate constants (k) were obtained from the PC oxidation curves by using the equation $ln(A_0/A) = kt$, where *t* is the reaction time. In the absence of PNCs, the photolytic reaction did not cause a significant decrease in the A/A_0 ratio, with a new signal emerging progressively at ~280 nm. We corroborated the photochemical conversion of some BzOH molecules to benzaldehyde (BzCHO) by comparing the typical UV-Vis absorption spectra of this organic compound over the time. Then, by introducing the photocatalysts, the initial absorbance increased ~10 times compared to the initial value under photolytic conditions, and a broader peak was formed. This feature has been associated with the interaction between silanol groups (-Si-OH) from silica and the BzOH species, resulting in covalent Si-O-C type interactions.⁴⁹ Accordingly, we propose for the first time a synergistic mechanism provided by the SiO_x shell covering the PQDs during the PC reaction, restraining the fast diffusion of EtOH molecules to the PQD core at the initial stage, while promoting the BzOH chemisorption through the silanol moieties on the photocatalyst surface. Under this premise, the oxidation of the organic molecule on the PQDs@SiOx/solution interface can be facilitated. Finally, with the aim of studying the influence of the EtOH medium on the PC performance of PQDs, we conducted the PC BzOH oxidation in the presence of acetonitrile (replacing EtOH), determining that no signals of BzOH chemisorption or the formation of BzCHO were obtained after 100 min, see Fig. S16. This indicates that EtOH modifies the PQD surface through the

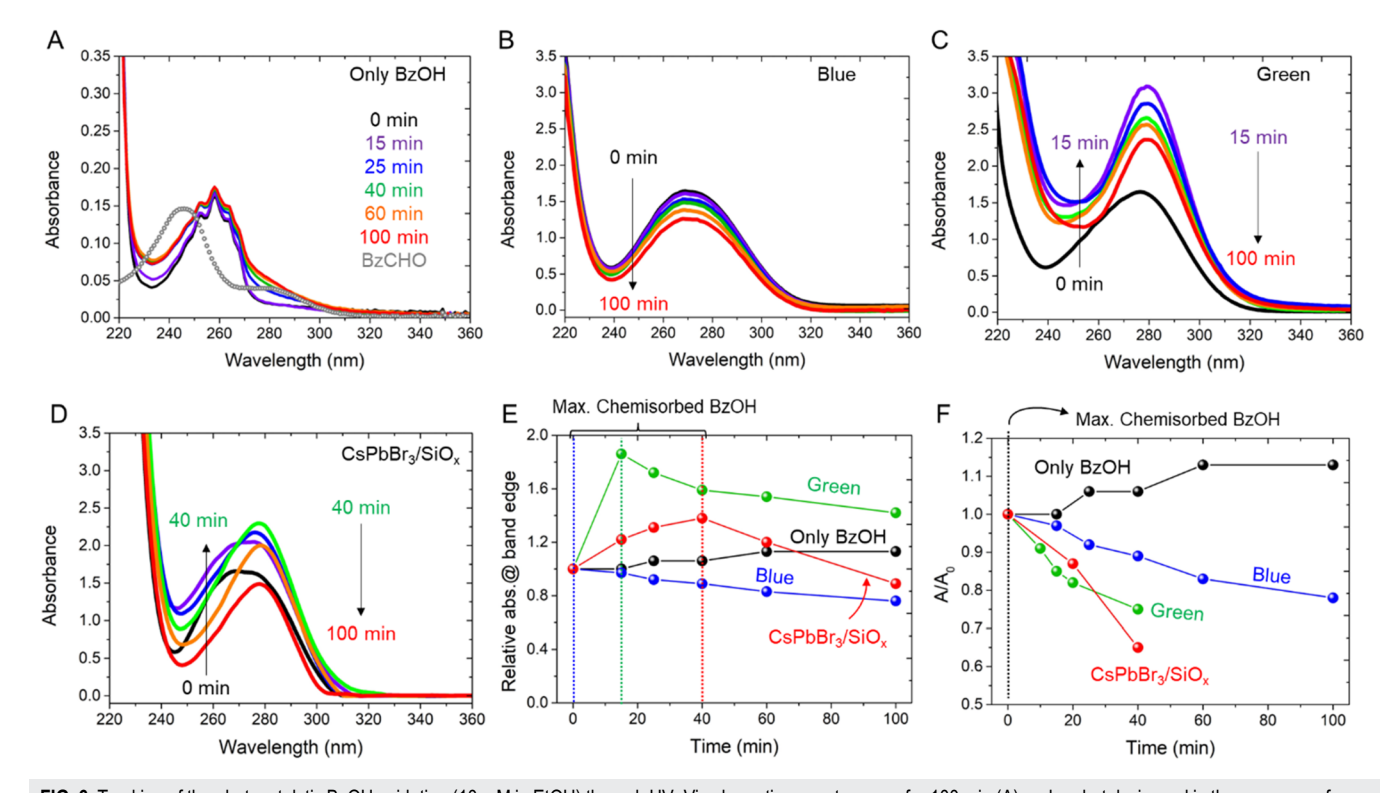


FIG. 6. Tracking of the photocatalytic BzOH oxidation (10 mM in EtOH) through UV–Vis absorption spectroscopy for 100 min (A) under photolysis, and in the presence of asprepared (B) Blue, (C) Green, and (D) CsPbBr₃@SiO_x photocatalysts (5.0 mg ml⁻¹). (E) Relative absorbance measured at the absorption band edge. (F) Photodegradation of benzyl alcohol (BzOH, 5 mM) vs time after reaching the maximum BzOH chemisorption.

generation of -Si-OH species, which is a key factor in promoting the PC activity of photoactive materials.

On the other hand, we observed a progressive increase of the absorption intensity in the PQD@SiOx as follows: Blue < CsPbBr₃@SiO_x < Green. Given that SiO_x media formation is similar for all the PQDs, the difference in the ability to favor BzOH chemisorption can be related to the amount of SiO_x covering the PNCs with higher particle sizes (Green > CsPbBr₃@SiO_x > Blue). Thus, we believe that the content of silanol groups in the PQD@SiO_x composite increases with the use of larger PNCs, lowering the time required to favor maximum BzOH chemisorption mediated by Green MA_vCs_{1-v}PbX₃ PQD@SiO_x, see Fig. 6(E). Interestingly, this characteristic is not proportional to the highest PC performance for BzOH oxidation, which was established for the CsPbBr₃@SiO_x PQDs, see Fig. 6(F). This material achieved the highest photocatalytic efficiency [denoted as the percentage of oxidized BzOH ($A/A_0 \times 100$), after completing the PC oxidation reaction (100 min)] of ~35%, followed by MA_yCs_{1-y}PbBr₃@SiO_x PQDs and MA_yCs_{1-y}PbCl_{3-x}Br_x@SiO_x PQDs with values of ~25% and 22%, respectively. Furthermore, as seen in Fig. S17, the CsPbBr₃@SiO_x PQD system produces the fastest BzOH consumption by photogenerated holes at the photocatalyst/solution interface (highest k), which agrees with the highest PC performance. Later, we analyzed the photocatalyst reusability by conducting the PC BzOH oxidation for two more reaction cycles (three reaction cycles in total), adding the recovered PQDs into a new BzOH ethanolic solution, see Figs. S18(A) and S18(B). For this purpose, we chose the MA_yCs_{1-y}PbBr₃@SiO_x PQDs due to this material facilitating maximum BzOH chemisorption in a short time. Unlike the first cycle, where BzOH chemisorption and subsequent oxidation were favored, well-defined absorption signals attributed to the presence of BzOH and BzCHO at 252 and 282 nm, respectively, were evidenced after the second and third cycles. Interestingly, the second cycle exhibits a progressive increase in the BzCHO signal after 100 min of PC reaction, without decreasing the BzOH absorption, while the respective BzOH and BzCHO signals do not show any change in absorption intensity after the third cycle. In light of these results, we propose a PC mechanism where -Si-OH moieties generated by the presence of EtOH interact with BzOH molecules through Si-O-C interactions during the first cycle. Here, photogenerated holes mediate BzOH oxidation to produce mainly BzCHO, as evidenced after the second and third cycles. However, the fact that the BzOH signal is no longer decreased during the PQD reusability, even losing the PC activity for BzCHO formation allows to suggest that the SiO_x layer is deteriorated under the alcohol medium along the time. This is expected since the amount of alcohol can alter the hydrolysis and condensation reaction equilibrium for SiO_x shell formation, generating an inhomogeneous SiO_x layer covering the PQDs.

The deterioration of the SiO_x shell was confirmed by detecting Pb^{2+} leaching into the ethanolic BzOH solution after the three PC reactions. For this purpose, we added 10 mM MAI in EtOH to the collected solutions from each cycle, observing the formation of PbI_2 precipitate. Then, using the molar mass of PbI_2 , the Pb^{2+} molarity of the collected solutions was determined to be 3.9 mM (first cycle), 3.5 mM (second cycle), and 3.9 mM (third cycle). Thus, we conclude that the SiO_x shell is no longer protecting the PQDs under an EtOH environment, causing degradation of the photoactive material and thereby the loss of its PC performance. At this

point, although we are still determining suitable conditions to obtain a more robust and homogeneous SiO_x coverage for protecting the PQDs for a longer time in alcohol environments, we deduce that the incorporation of MAX through one-pot synthesis or carrying out a post-synthetic halide exchange process promotes the formation of a less-defective $MA_yCs_{1-y}PbX_3$ PQDs@SiO_x structure, with a controllable bandgap, improved color quality, and suitable oxidizing power for triggering the PC degradation of BzOH as a proof-of-concept, which is attractive for future optoelectronics and solar-driven PC technologies.

III. CONCLUSIONS

In this work, we introduced two different synthetic routes, such as one-pot and post-synthetic approaches, for the preparation of MA_vCs_{1-v}PbX₃ PQDs@SiO_x with a tunable bandgap and a high-quality color gamut. By adding MAX to the initially highly defective CsPbBr₃@SiO_x structure, the compensation of the A-site defects is favored by the presence of MA⁺ cations filling Cs⁺ vacancies, improving the surface stoichiometry of the resultant materials. In this context, the radiative channel for carrier recombination was enhanced, decreasing the likelihood of carrier trapping. Simultaneously, the MAX incorporation allows the modulation of the photophysical features of the PQDs@SiO_x, indicating the imperfect protective coverage provided by the silica shell. However, once a post-synthetic annealing is applied, the anion exchange between the prepared PQDs@SiO_x is restrained, allowing the generation of white color emission with a color stability of 60 minutes. Finally, the postannealed PQDs@SiOx are suitable for triggering the photocatalytic degradation of BzOH under UV-Vis irradiation, showing a compromise between the chemisorption process (given by the Si-O-C interactions of BzOH molecules and SiO_x coverage) and the highly oxidizing power produced by the PQD core. In this way, the photomaterials promoted BzOH photodegradation with a maximum efficiency of 35% in an EtOH environment, also exhibiting the stability of photocatalysts in polar media. Accordingly, less-defective MA_yCs_{1-y}PbX₃ PQDs@SiO_x can be considered good candidates for incorporating into future optoelectronic and emerging solar-driven technologies.

SUPPLEMENTARY MATERIAL

The supplementary material describes the experimental setup. Results include high-resolution (HR) TEM images and corresponding particle size distribution, x-ray diffraction data, FT-IR, HR-XPS absorption/PL emission spectra, and PL stability of MA_yCs_{1-y}PbX₃@SiO_x PQDs, PL performance of PQD-based color-converting LEDs, and PC activity of PQD photocatalysts during their reusability.

ACKNOWLEDGMENTS

This work was supported by the National Research Foundation of Korea grant funded by the Korean government (Grant Nos. 2022R1C1C1011860, RS-2024-00441659). This work was partially funded by MCIN with funding from the European Union NextGenerationEU (Grant No. PRTR-C17.I1) through project

PLEDS (Grant No. PID2022-140090OB) and by the project Q-Solutions (Grant No. CIPROM/2021/078) funded by the Generalitat Valenciana via PROMETEO. A.F.G.R. thanks ANID for financial support through the FONDECYT Iniciación Project (Grant No. 11240161), and through the Vinculación International Project (Grant No. FOV240255). S.J.Y. and J.P. also acknowledge the Korea Basic Science Institute (National Research Facilities and Equipment Center) grant funded by the Ministry of Education (Grant No. 2020R1A6C101B194) for utilizing characterization tools.

AUTHOR DECLARATIONS

Conflict of Interest

The authors have no conflicts to disclose.

Author Contributions

S.S., H.J., and Y.K. contributed equally to this work

S.J.L. and S.J.Y. proposed an overall study. S.J.L., S.S., H.J., Y.K., and S.J.Y. designed the experiments. S.J.L., S.S., H.J., Y.J.L., S.Y.P., Y.K., and S.M. synthesized the PQDs. S.S., S.J.L., H.J., E.Y.C., Y.J.L., and Y.K. conducted the optical, morphological, structural, and surface chemistry characterization. I.M.S., A.F.G.R., and S.J.Y. led overall research directions and financial support. All authors contributed to writing the manuscript and the discussions.

Sumi Seo: Conceptualization (lead); Data curation (equal); Formal analysis (lead); Investigation (equal); Methodology (equal); Supervision (lead); Validation (lead); Visualization (lead); Writing - original draft (lead); Writing - review & editing (lead). Hyeonyeong Jo: Data curation (equal); Formal analysis (equal); Investigation (equal); Methodology (equal). YoonGyo Kim: Data curation (equal); Formal analysis (equal); Investigation (equal); Methodology (equal). Eun Young Choi: Data curation (supporting); Formal analysis (supporting); Investigation (supporting); Methodology (supporting). Soo Jeong Lee: Data curation (supporting); Formal analysis (supporting); Investigation (supporting); Methodology (supporting). Kayoung Cho: Data curation (supporting); Formal analysis (supporting); Investigation (supporting); Methodology (supporting). Sohee Mo: Data curation (supporting); Formal analysis (supporting); Investigation (supporting); Methodology (supporting). You Jeong Lee: Data curation (supporting); Formal analysis (supporting); Investigation (supporting); Methodology (supporting). Seong Yeon Park: Data curation (supporting); Formal analysis (supporting); Investigation (supporting); Methodology (supporting). Jin Ho Bang: Conceptualization (lead); Data curation (supporting); Formal analysis (lead); Investigation (lead); Methodology (lead); Visualization (lead); Writing - review & editing (lead). Iván Mora-Seró: Conceptualization (equal); Formal analysis (equal); Funding acquisition (equal); Investigation (equal); Methodology (equal); Project administration (equal); Validation (equal); Visualization (lead); Writing - review & editing (equal). Andrés F. Gualdrón-Reyes: Conceptualization (equal); Data curation (equal); Formal analysis (equal); Funding acquisition (equal); Investigation (equal); Methodology (equal); Project administration (equal); Supervision (equal); Validation (equal); Visualization (equal); Writing - original draft (equal); Writing – review & editing (equal). JaeHong Park: Data curation (equal); Formal analysis (equal); Investigation (equal); Project administration (equal); Validation (equal); Writing – review & editing (equal). Seog Joon Yoon: Conceptualization (lead); Data curation (lead); Formal analysis (lead); Funding acquisition (lead); Investigation (lead); Methodology (lead); Project administration (lead); Resources (lead); Supervision (lead); Validation (lead); Visualization (lead); Writing – original draft (lead); Writing – review & editing (lead).

DATA AVAILABILITY

The data that support the findings of this study are available within the article and its supplementary material and are openly available in the Zenodo repository at https://doi.org/10.5281/zenodo.15548240.⁴⁵

REFERENCES

- ¹Y.-S. Chen, J. S. Manser, and P. V. Kamat, J. Am. Chem. Soc. **137**(2), 974–981 (2015).
- ²C. Lee, Y. Shin, A. Villanueva-Antolí, S. Das Adhikari, J. Rodriguez-Pereira, J. M. Macak, C. A. Mesa, S. Giménez, S. J. Yoon, A. F. Gualdrón-Reyes, and I. Mora-Seró, Chem. Mater. 33(22), 8745–8757 (2021).
- ³S. A. Veldhuis, P. P. Boix, N. Yantara, M. Li, T. C. Sum, N. Mathews, and S. G. Mhaisalkar, Adv. Mater. 28, 6804 (2016).
- ⁴J. De Roo, M. Ibáñez, P. Geiregat, G. Nedelcu, W. Walravens, J. Maes, J. C. Martins, I. Van Driessche, M. V. Kovalenko, and Z. Hens, ACS Nano **10**(2), 2071–2081 (2016).
- ⁵ A. Dey, J. Ye, A. De, E. Debroye, S. K. Ha, E. Bladt, A. S. Kshirsagar, Z. Wang, J. Yin, Y. Wang, L. N. Quan, F. Yan, M. Gao, X. Li, J. Shamsi, T. Debnath, M. Cao, M. A. Scheel, S. Kumar, J. A. Steele, M. Gerhard, L. Chouhan, K. Xu, X.-g. Wu, Y. Li, Y. Zhang, A. Dutta, C. Han, I. Vincon, A. L. Rogach, A. Nag, A. Samanta, B. A. Korgel, C.-J. Shih, D. R. Gamelin, D. H. Son, H. Zeng, H. Zhong, H. Sun, H. V. Demir, I. G. Scheblykin, I. Mora-Seró, J. K. Stolarczyk, J. Z. Zhang, J. Feldmann, J. Hofkens, J. M. Luther, J. Pérez-Prieto, L. Li, L. Manna, M. I. Bodnarchuk, M. V. Kovalenko, M. B. J. Roeffaers, N. Pradhan, O. F. Mohammed, O. M. Bakr, P. Yang, P. Müller-Buschbaum, P. V. Kamat, Q. Bao, Q. Zhang, R. Krahne, R. E. Galian, S. D. Stranks, S. Bals, V. Biju, W. A. Tisdale, Y. Yan, R. L. Z. Hoye, and L. Polavarapu, ACS Nano 15(7), 10775–10981 (2021).
- ⁶R. Grisorio, M. E. Di Clemente, E. Fanizza, I. Allegretta, D. Altamura, M. Striccoli, R. Terzano, C. Giannini, M. Irimia-Vladu, and G. P. Suranna, Nanoscale 11(3), 986–999 (2019).
- ⁷R. Grisorio, D. Conelli, R. Giannelli, E. Fanizza, M. Striccoli, D. Altamura, C. Giannini, I. Allegretta, R. Terzano, and G. P. Suranna, Nanoscale **12**(32), 17053–17063 (2020).
- ⁸J. S. Manser, J. A. Christians, and P. V. Kamat, Chem. Rev. **116**(21), 12956–13008 (2016).
- ⁹E. Scharf, F. Krieg, O. Elimelech, M. Oded, A. Levi, D. N. Dirin, M. V. Kovalenko, and U. Banin, Nano Lett. **22**(11), 4340–4346 (2022).
- ¹⁰G. Nedelcu, L. Protesescu, S. Yakunin, M. I. Bodnarchuk, M. J. Grotevent, and M. V. Kovalenko, Nano Lett. 15(8), 5635–5640 (2015).
- ¹¹J. Song, O. Wang, H. Shen, Q. Lin, Z. Li, L. Wang, X. Zhang, and L. S. Li, Adv. Funct. Mater. 29(33), 1808377 (2019).
- ¹²W. Bai, T. Xuan, H. Zhao, H. Dong, X. Cheng, L. Wang, and R. J. Xie, Adv. Mater. 35(39), 2302283 (2023).
- ¹³H. Aqoma, S.-H. Lee, I. F. Imran, J.-H. Hwang, S.-H. Lee, and S.-Y. Jang, Nat. Energy 9(3), 324–332 (2024).
- ¹⁴S. Min, M. Jeon, J. Cho, J. H. Bang, and P. V. Kamat, Nano Convergence 11(1), 49 (2024).
- ¹⁵V. Malgras, S. Tominaka, J. W. Ryan, J. Henzie, T. Takei, K. Ohara, and Y. Yamauchi, J. Am. Chem. Soc. 138(42), 13874–13881 (2016).

- ¹⁶V. Malgras, J. Henzie, T. Takei, and Y. Yamauchi, Chem. Commun. 53(15), 2359–2362 (2017).
- ¹⁷V. Malgras, J. Henzie, T. Takei, and Y. Yamauchi, Angew. Chem., Int. Ed. 57(29), 8881–8885 (2018).
- ¹⁸ X. Tang, J. Yang, S. Li, Z. Liu, Z. Hu, J. Hao, J. Du, Y. Leng, H. Qin, X. Lin, Y. Lin, Y. Tian, M. Zhou, and Q. Xiong, Adv. Sci. 6(18), 1900412 (2019).
- ¹⁹Z. Li, L. Kong, S. Huang, and L. Li, Angew. Chem., Int. Ed. **56**(28), 8134–8138 (2017)
- ²⁰G. Yang, Q. Fan, B. Chen, Q. Zhou, and H. Zhong, J. Mater. Chem. C 4(48), 11387–11391 (2016).
- ²¹ Z. Zhang, L. Liu, H. Huang, L. Li, Y. Wang, J. Xu, and J. Xu, Appl. Surf. Sci. 526, 146735 (2020).
- ²²P. R. Bommireddy, J. Babu B, S. Sunku, K. Basha C, Y. Suh, C. Sekhar M, and S.-H. Park, Heliyon **10**(2), e24497 (2024).
- ²³ S. Y. Park, G. Seo, T. Kim, C. Pareja-Rivera, F. Pino, Y. G. Kim, J. Simancas, B. Kim, I. Utreras-Asenjo, J. Rodriguez-Pereira, H. Jo, J. H. Park, J. H. Bang, S. Masi, S. J. Yoon, I. Mora-Seró, and A. F. Gualdrón-Reyes, Adv. Optical Mater. e00968 (published online 2025).
- (published online 2025).

 24 K. Cho, Y. Park, H. Jo, S. Seo, J. Moon, S. J. Lee, S. Y. Park, S. J. Yoon, and J. Park, J. Phys. Chem. Lett. 15(21), 5795–5803 (2024).
- ²⁵ S. J. Lee, Y. J. Lee, S. Seo, H. Jo, D. Han, and S. J. Yoon, Bull. Korean Chem. Soc. 43(12), 1312–1319 (2022).
- ²⁶S. Han, Y. Ji, and Y. Li, Nanoscale **17**(11), 6793–6803 (2025).
- ²⁷ M. Roy, Vikram, S. Banerjee, A. Mitra, A. Alam, and M. Aslam, Chem. Eur. J. 25(42), 9892–9901 (2019).
- ²⁸ H. Jeon, H. Jo, S. Seo, S. J. Lee, S. J. Yoon, and D. Han, Sens. Actuators Rep. **8**, 100208 (2024).
- ²⁹ S. R, V. Nayak, M. S. Jyothi, and R. Geetha Balakrishna, J. Alloys Compd. 834, 155246 (2020).
- ³⁰ N. Pellet, J. Teuscher, J. Maier, and M. Grätzel, Chem. Mater. **27**(6), 2181–2188 (2015).
- ³¹S. J. Yoon, S. Draguta, J. S. Manser, O. Sharia, W. F. Schneider, M. Kuno, and P. V. Kamat, ACS Energy Lett. 1(1), 290–296 (2016).
- ³²J. Yin, H. Yang, K. Song, A. M. El-Zohry, Y. Han, O. M. Bakr, J.-L. Brédas, and O. F. Mohammed, J. Phys. Chem. Lett. **9**(18), 5490–5495 (2018).
- ³³X. Shen, K. Kang, Z. Yu, W. H. Jeong, H. Choi, S. H. Park, S. D. Stranks, H. J. Snaith, R. H. Friend, and B. R. Lee, Joule 7(2), 272–308 (2023).

- ³⁴S. J. Lee, Y. J. Lee, S. Seo, H. Jeon, D. Han, H. Im, N. K. Shrestha, and S. J. Yoon, J. Phys. Chem. C **126**(18), 7910–7921 (2022).
- ³⁵ A. Maqsood, Y. Li, J. Meng, D. Song, B. Qiao, S. Zhao, and Z. Xu, Nanoscale Res. Lett. 15(1), 89 (2020).
- ³⁶ K. Kim, Y. Shin, C. Lee, H. Jeon, S. J. Yoon, and D. Han, Analyst **147**(5), 841–850 (2022).
- ³⁷T. C. A. da Silva, C. Fernández-Saiz, R. S. Sánchez, A. F. Gualdrón-Reyes, I. Mora-Seró, and B. Julián-López, J. Sol-Gel Sci. Technol. 114, 131 (2025).
- ³⁸R. Yadav, M. Roy, G. Banappanavar, and M. Aslam, Chem. Asian J. **17**(7), e202200087 (2022).
- ³⁹S. Masi, A. F. Gualdrón-Reyes, and I. Mora-Seró, ACS Energy Lett. 5(6), 1974–1985 (2020).
- ⁴⁰S. Maity, V. K. Lokku, A. Lata, K. Sarkar, J. Ahmed, M. A. Majeed Khan, and P. Kumar, Indian J. Phys. **96**(3), 903–908 (2022).
- ⁴¹ X. Hou, S. Huang, W. Ou-Yang, L. Pan, Z. Sun, and X. Chen, ACS Appl. Mater. Interfaces 9(40), 35200–35208 (2017).
- ⁴²C. Jo, D. Kim, C.-L. Lee, and D.-K. Ko, Opt. Express **31**(24), 40352 (2023).
- ⁴³ J. Lee, M. H. Naveen, J. Park, K. Pyo, H. Kim, D. Lee, and J. H. Bang, ACS Energy Lett. **6**(6), 2305–2312 (2021).
- ⁴⁴T.-Y. Kim, B. S. Kim, J. G. Oh, S. C. Park, J. Jang, T. W. Hamann, Y. S. Kang, J. H. Bang, S. Giménez, and Y. S. Kang, ACS Appl. Mater. Interfaces 13(5), 6208–6218 (2021).
- ⁴⁵ A. F. Gualdrón-Reyes, S. Masi, and I. Mora-Seró, Trends Chem. **3**(6), 499–511 (2021).
- ⁴⁶X. Shen, Y. Zhang, S. V. Kershaw, T. Li, C. Wang, X. Zhang, W. Wang, D. Li, Y. Wang, M. Lu, L. Zhang, C. Sun, D. Zhao, G. Qin, X. Bai, W. W. Yu, and A. L. Rogach, Nano Lett. **19**(3), 1552–1559 (2019).
- ⁴⁷W. Li, F. Chun, X. Fan, W. Deng, M. Xie, C. Luo, S. Yang, H. Osman, C. Liu, and W. Yang, J. Mater. Sci. 54(5), 3786–3794 (2018).
- ⁴⁸Q. Zhong, M. Cao, H. Hu, D. Yang, M. Chen, P. Li, L. Wu, and Q. Zhang, ACS Nano 12(8), 8579–8587 (2018).
- ⁴⁹V. B. Arce, S. G. Bertolotti, F. J. V. E. Oliveira, C. Airoldi, A. Arques, L. Santos-Juanes, M. C. Gonzalez, C. J. Cobos, P. E. Allegretti, and D. O. Mártire, Photochem. Photobiol. Sci. 11(6), 1032–1040 (2012).